Xue, Bing; Haneda, Katsuyuki; Icheln, Clemens; Vähä-Savo, Lauri

Comparison of Measured and Simulated Radiation from 5G Cellphone Antennas with Hand Phantoms

Published in:
17th European Conference on Antennas and Propagation, EuCAP 2023

DOI:
10.23919/EuCAP57121.2023.10133751

Published: 01/01/2023

Document Version
Peer-reviewed accepted author manuscript, also known as Final accepted manuscript or Post-print

Comparison of Measured and Simulated Radiation from 5G Cellphone Antennas with Hand Phantoms

Bing Xue*, Katsuyuki Haneda*, Clemens Icheln*, Lauri Vähä-Savo*
*Department of Electronics and Nanoengineering, Aalto University-School of Electrical Engineering, Espoo, Finland, E-mail: bing.xue@aalto.fi

***Abstract*—In this manuscript, hand effects on cellphone antennas at 5G millimeter-wave frequencies are evaluated through measurements using hand phantoms and are compared with results from electromagnetic simulations. First, two configurations of a dual-polarized 4-element linear antenna array operating at 28 GHz are introduced. One-hand and two-hand physical phantoms and their numerical models for electromagnetic simulations are illustrated. Then, the array evaluation metric, i.e., spherical coverage, is introduced to assess statistics of realized gain across the solid angle. Next, antenna measurement setups are implemented for the two antenna arrays combined with the two physical hand phantoms. Finally, the spherical coverage and the corresponding cumulative distribution function are calculated. Differences in the realized gains derived from simulated and measured antenna arrays are about 1 dB at the median levels of the cumulative distribution. The differences are comparable to those observed when real hands are used in measurements instead of phantom hands [1].**

***Index Terms*—Cellphone antenna array, millimeter-wave, spherical coverage, hand phantom, user impacts.**

I. Introduction

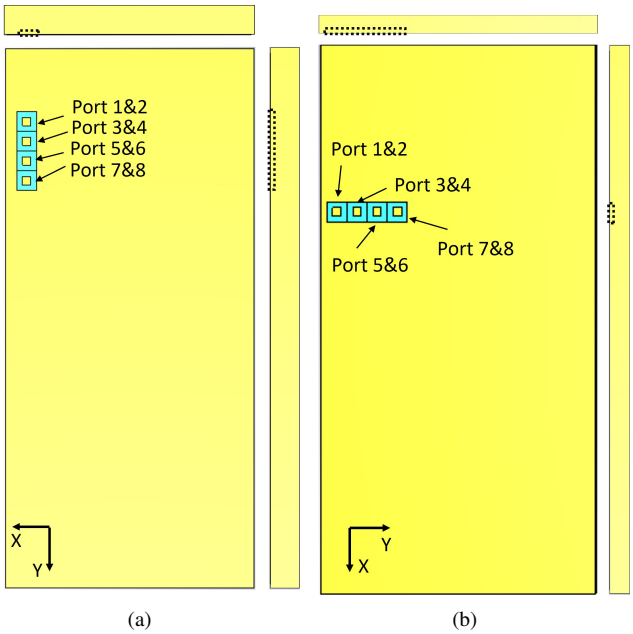

(a) (b)

Fig. 1. 28 GHz antenna array configurations from the top views and the side views of a metal phone chassis (two discrete ports per antenna element, 8 ports in total); (a) portrait mode and (b) landscape mode.

Millimeter-wave (mmW) wireless communication has been a research hotspot in recent years due to its high date-rate potential. Achieving robust operations in a dynamic environment brings about more design challenges in frequency band 2 (FR2), i.e., 24.5 to 43 GHz, than in FR1 covering the sub-6 GHz band. The user's body reflects and absorbs electromagnetic waves especially in the mmW bands, causing detrimental changes in radiation properties of cellphone antennas. Figuring out their effect is therefore a key issue in the community of cellphone antenna design. Plenty of papers focus on interactions between antennas and human bodies for above-6 GHz bands [2]–[8]. Most of them discuss combined effects of human bodies and hands. A fewer number of papers investigated the effect of hands as a separate entity from body, including the finger effects [9], [10] and the whole hands' effects [11]–[14]. All these works, however, *lack comparisons between simulations and measurements* for cross-validations of the simulation models and measurement methods. When simulation reproduces the measurement with sufficient accuracy, we do not have to do measurements for every new prototype of 5G mmW cellphone antenna arrays. One significant step to the cross-validation is reported in [1], where the measured radiation characteristics of an mmW cellphone array with a human body influence were compared with corresponding electromagnetic simulations. In [1] the antenna-hand interaction measurements were realised with near-field scanning and near-field-to-far-field transformation. That approach suffered from 1) the non-repeatable posture of a real human hand during measurements and 2) the limited angular range of near-field observation (only 33.4% of the solid angle). Therefore, in this paper, we utilize hand phantoms to evaluate the uncertainty of the measurement method more properly where 1) the measurements are repeatable and 2) the far-field observation covers the whole solid angle. Furthermore, in addition to the spherical coverage, evaluation metrics in this paper also include the radiation patterns of each antenna-array element.

II. Millimeter-wave Cellphone Antenna Array Configurations

Simple linear antenna array models, shown in Fig. 1, are used to study hand effects on its radiation performances by full-wave simulations. The two 4-element antenna arrays working at 28 GHz for landscape and portrait modes are embedded in the copper chassis. The designed antenna elements

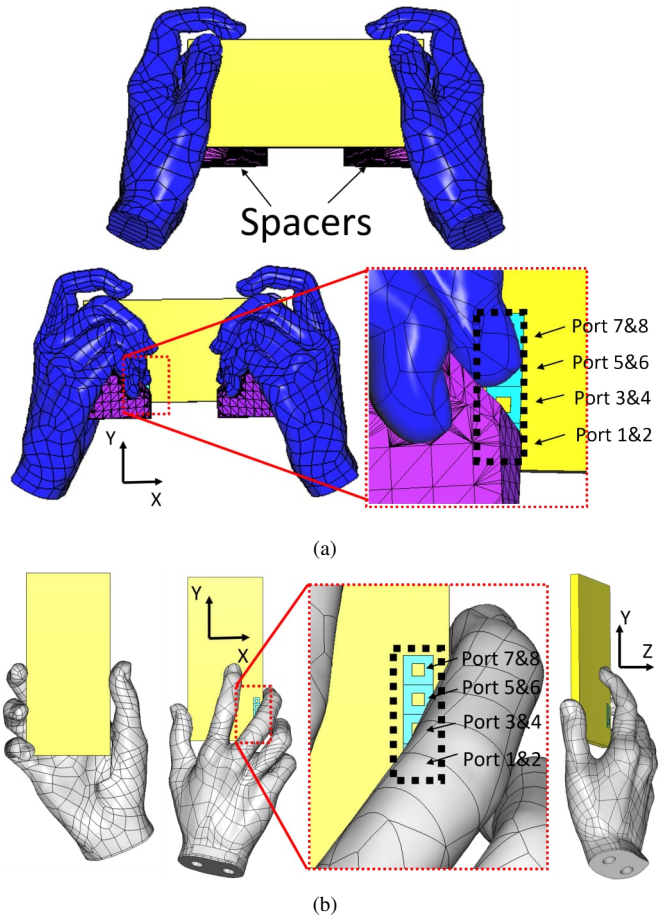

Fig. 2. Different views of (a) the two-hand-phantom and (b) one-hand-phantom numerical models with a cellphone chassis. The black dotted rectangle shows the array location

are stacked patches. The top and bottom substrates are 0.5 and 0.1 mm, respectively. Details of the antenna element and stack-up design of the phone mockup are available in [1]. The size of the antenna array is 5×20 mm^2. The distance between two elements is 5 mm. A discrete port is used as the excitation source for each antenna. For practical reasons to fit the mockups into hand phantoms, the scale of the cellphone chassis is chosen as $69\times150\times8$ mm^3 for the portrait mode and $75 \times 150 \times 5$ mm^3 for the landscape mode, respectively. The port indices i corresponding to the two mockups are shown in Fig. 1. Even/odd indices possess the same polarization.

III. Hand Phantoms and Models

In this paper, we adopt two kinds of numerical hand models, namely the two-hand model (landscape mode) and the one-hand model (portrait mode). Those two modes correspond to the hand phantoms from the *speag* company. In both phantoms, the surface is coated with a special material that has a permittivity close to that of a real hand in mmW frequencies. Since we do not know the exact permittivity values of the phantom skin material at 28 GHz, we assume that they are identical to the canonical human skin's permittivity and conductivity, i.e., $\epsilon_{\mathrm{r}} = 16.55$ and $\sigma = 25.82$ S/m [9]. Figure 2 shows the different views of the one- and two-hand phantoms with the cellphone chassis. Spacers are set between the two-hand phantom and chassis to fix them tight. Impacts of the spacers on radiation characteristics of the antenna arrays are negligible since their permittivity is close to air. The following simulations were implemented in *CST Studio Suite* via the time-domain method. The hand models and the cellphone chassis were meshed by $1/10$ wavelengths of 28 GHz without using the mesh refinement technique, while the antenna-array parts were meshed more densely. In this way, the simulation time is manageable.

(a) (b)

Fig. 3. The measurement setup of (a) portrait mode and (b) landscape mode

IV. Evaluation Metrics

Radiation patterns are utilized to assess the performance of antennas and as a metric to compare the simulation results and the experimental ones. In addition, spherical coverage is deemed as a good benchmark to assess the statistical characteristic of the array gain, which relies on the empirical statistic of the maxima of gains for each angle on a sphere. In this manuscript, pattern syntheses are based on the same way as [6]. Moreover, the cumulative distribution function (CDF) of spherical coverage is also calculated to assess antenna's performances in an intuitive way. For each angle $\mathbf{\Omega} = (\theta, \phi)$, the maximum realized gain of the array can be expressed as [6]

$$\hat{G}(\mathbf{\Omega}) = \max_k G_k(\mathbf{\Omega}), \tag{1}$$

where $G_k(\mathbf{\Omega}) = \|\boldsymbol{E}_k(\mathbf{\Omega})\|^2$ is the realized gains of an antenna array's k-th beam synthesized patterns; $\boldsymbol{E}_k(\mathbf{\Omega}) = [E_\theta(\mathbf{\Omega})\ E_\phi(\mathbf{\Omega})]$ is the complex gain vector; $1 \le k \le 512$ is the number of beams we considered. Then, its CDF can be defined by

$$CDF(x) = \mathrm{prob}(\hat{G} < x), \tag{2}$$

where $\mathrm{prob}(\cdot)$ is a probability operator yielding values $\in [0, 1]$. While conducting the spherical coverage statistics, angles $\mathbf{\Omega}$ should be uniform on the whole sphere so that any adjacent points on the sphere have the same spacing in the solid angle [15]. In the paper, the number of equidistant sampling points of gains over a sphere is 10000.

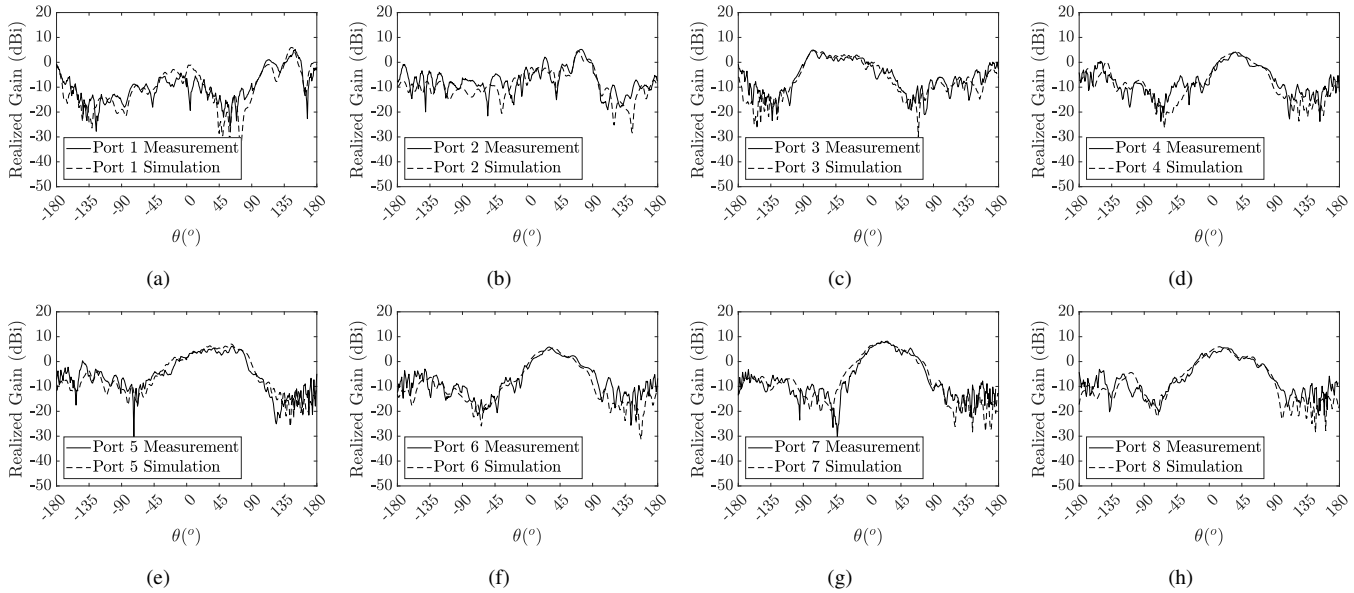

Fig. 4. The maximum realized gains over the pole angle (θ) for (a) Port 1, (b) Port 2, (c) Port 3, (d) Port 4, (e) Port 5, (f) Port 6, (g) Port 7, and (h) Port 8 of portrait mode at 28GHz ($\theta \in [-180^\circ\ 180^\circ]$ and $\phi \in [0^\circ\ 180^\circ]$).

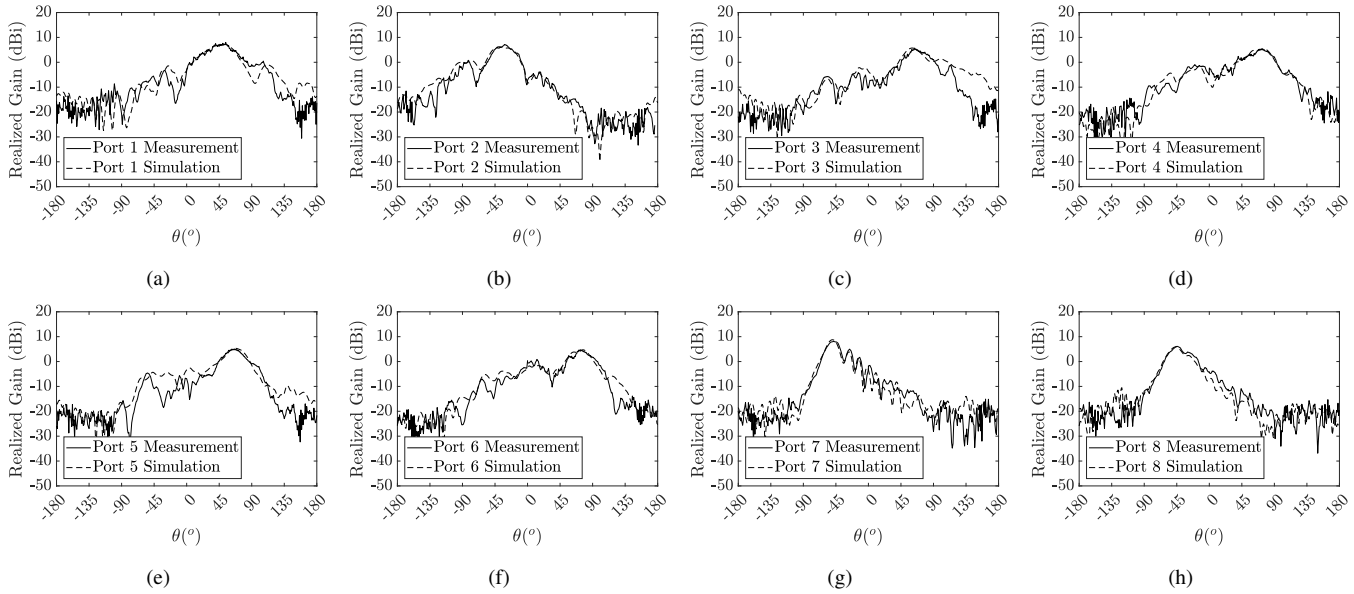

Fig. 5. The maximum realized gains over the pole angle (θ) for (a) Port 1, (b) Port 2, (c) Port 3, (d) Port 4, (e) Port 5, (f) Port 6, (g) Port 7, and (h) Port 8 of landscape mode at 28GHz ($\theta \in [-180^\circ\ 180^\circ]$ and $\phi \in [0^\circ\ 180^\circ]$).

V. Experimental Validation

Far-field measurements of prototyped antenna arrays, which are integrated with corresponding hand phantoms, are performed in an anechoic chamber. The prototypes are detailed in [1]. These far-field measurements have the following advantages over the near-field measurements with real human hands:

1) It is possible to analyze impacts of hands separately from their body; the near-field measurements with real humans do not allow straightforward separation of body and hand effects on antenna radiation.
2) It is possible to circumvent the non-repeatable nature of real human hands; the near-field measurements require a few minutes to complete them, within which the human cannot stay exactly still.

The far-field measurement setups with hand phantoms are shown in Fig. 3. 3D-printed fixtures made of low-permittivity materials were used to fix the phantoms on the testing tower. For the two-hand phantom, the center of the cellphone was set along the rotation axis of the testing tower, which was several centimeters away from the phase center of each antenna. It only caused $< 1^\circ$ deviation in the far-field observation angles

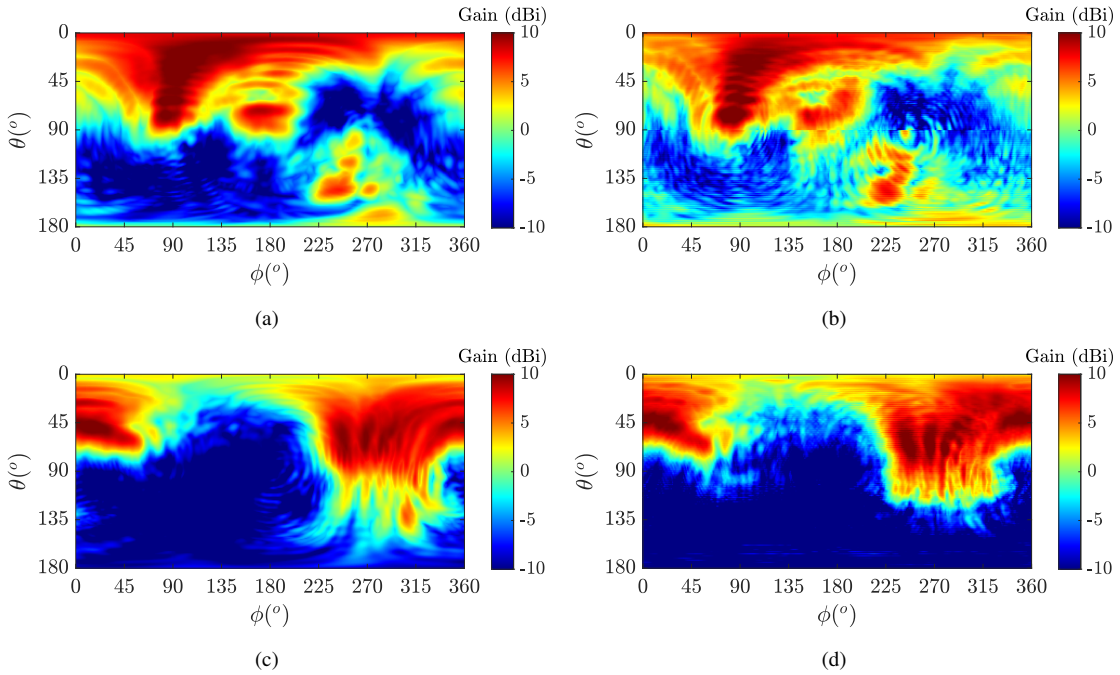

Fig. 6. Spherical coverage of (a) simulation results and (b) measurement results for the portrait mode at 28 GHz; Spherical coverage of (c) simulation results and (d) measurement results for the landscape mode at 28 GHz ($\theta \in [0^\circ\ 180^\circ]$ and $\phi \in [0^\circ\ 360^\circ]$).

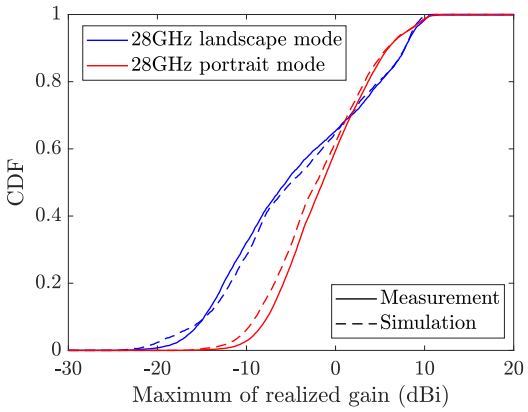

Fig. 7. The CDF of the spherical coverage.

because the receiving antenna was apart from the testing tower by 5.5 m. For the one-hand phantom, the antenna array was aligned with the rotation axis of the testing tower, allowing us to neglect the misalignment error in the field observation angles. The hand postures shown in Fig. 2 were implemented in the experiments for both the portrait and landscape modes. The fingers were 6 mm away from the antennas in the normal direction. Thus, there exist no noticeable detuning effects on the antennas at 28 GHz [10]. By observing simulation curves in Fig. 4 and in Fig. 5, we can easily see that large $\theta \leq 160^\circ$ resulted in a high gain for portrait mode but a low gain for landscape mode. The absorber installed on the back of hand phantoms dramatically decreases the electromagnetic wave power in measurements. Therefore, in order to measure accurate power levels at large θ angles for portrait mode, the radiation patterns of each element were measured by the angle sweep setup ($\theta \in [0^\circ, 90^\circ]$, $\phi \in [0^\circ, 360^\circ]$), as shown in Fig. 3(a), and after the one-hand phantom was rotated by 180° along the y axis, we obtained power values at angles ($\theta \in [91^\circ, 180^\circ]$, $\phi \in [0^\circ, 360^\circ]$). On the other hand, for the landscape mode, the radiation patterns corresponding to all θs were measured by the setups shown in Fig. 3(b) only since the measurement error at large θs due to the absorber can be ignored. When installing the cellphone mock-ups on the phantoms, rulers were utilized to ensure that their relative position is consistent with that in the simulation. The measurement tower was rotated to obtain far-field observation angles at every $\phi = 1^\circ$ and $\theta = 2^\circ$, respectively. The output power and the intermediate-frequency bandwidth were set as 5 dBm and 1 kHz in *Keysight* N5227A vector network analyzer, respectively.

After the measurements, the losses of feed lines and connectors of the antenna prototypes were de-embedded by the approach proposed by our previous works [1], [6]. After that, the maximum realized gains over θ are shown for each port in Fig. 4 and Fig. 5. The measured curves and simulated curves coincide well. The maximum-gain difference is smaller than 2.5 dB on average, probably due to miscellaneous errors in the measurement setup, e.g., slight inconsistency of relative positions of phantoms and array mock-ups between simulations and measurements. The spherical coverages of the portrait mode and the landscape mode are also illustrated in Fig. 6. They have a different range of θ angles compared to the radiation pattern cuts in Fig. 4 and Fig. 5. The radiation

pattern cuts are on a plane ($\phi = x^\circ$) of the spherical coordinate system where there exists the maximum value of the antenna's realized gain. Hence, we are combining the θ radiation pattern cuts at $\phi = x^\circ$ and $\phi = (x+180)^\circ$ or $\phi = (x-180)^\circ$, leading to twice the range of θ angles compared to those of spherical coverage. Comparing the simulated and measured spherical coverages of the portrait mode, their gain distributions over the angles fit well with each other. The major mismatches from the angular ranges of low-level gains for portrait mode are because the reflections from the imperfect installed absorber on the testing tower improved gains at low levels. Another kind of mismatching is high-gain distribution differences, corresponding to the red color parts in Fig. 4(b), which are because of the inevitable difference of the hand posture between the numerical model and practical hand phantoms. Regarding landscape mode, the gain differences are mainly at the high θ range due to the fact that the installed absorber on the testing tower absorbed electromagnetic powers. Without a doubt, there is the same reason as portrait mode for the high-gain distribution differences. When it comes to the CDF of the spherical coverages shown in Fig.7. The major difference between simulated and measured CDF is $<$ 1.0 dB at the median level for both hand phantoms. The simulated spherical coverage for the antenna arrays at the landscape mode agrees well with that from measurements within the range $\theta < 125^\circ$. Radiations corresponding to large θ angles were attenuated by the existence of absorbers. Accordingly, the major difference between simulated and measured CDF is $<$ 1.3 dB at the low CDF levels.

When comparing with the CDF differences between the real-hand measurements and the corresponding simulations in [1], we can find that the CDF differences in this paper have similar levels in terms of low levels, median levels, and high levels. Both of them are around 1 dB.

VI. Conclusions

In this paper, we evaluate the uncertainty of antenna measurements with hand phantoms through spherical coverage of two antenna arrays and the radiation patterns of each antenna element. The maximum-gain difference is smaller than 2.5 dB on average for each antenna element. The median level of the spherical coverage CDF shows less than 1.0 dB difference between simulated and measured realized gains of the array in the portrait mode while that of landscape mode is less than 1.3 dB. Therefore, we can conclude that the measured results have a good agreement with the simulated ones. In our previous paper [1], a similar extent of agreement between CDF curves of the realized gain is observed between simulations and measurements, when considering non-repeatable real hands. It can demonstrate similar levels of uncertainty in spherical coverage for both repeatable measurements with hand phantoms and non-repeatable measurements with real hands in our antenna-hand interaction studies. We thereby prove the validity of our measurement method, regardless of whether it involves repeatable subjects or not. In the future, the numerical models of the antenna array and hands and their simulation setups can be adopted to evaluate and study hand effects at mmW frequencies, replacing practical experiments for a new mmW cellphone prototype.

Acknowledgments

The results presented in this paper have been partly supported by the Academy of Finland – NSF joint call pilot "Artificial intelligence and wireless communication technologies", decision # 345178.

References

[1] B. Xue, P. Koivumäki, L. Vähä-Savo, K. Haneda, and C. Icheln, "Impacts of real hands on 5G millimeter-wave cellphone antennas: Measurements and electromagnetic models," *arXiv e-prints*, p. arXiv:2208.01966, 2022.

[2] I. Syrytsin, S. Zhang, G. F. Pedersen, K. Zhao, T. Bolin, and Z. Ying, "Statistical investigation of the user effects on mobile terminal antennas for 5G applications," *IEEE Transactions on Antennas and Propagation*, vol. 65, no. 12, pp. 6596–6605, Dec. 2017.

[3] I. Syrytsin, S. Zhang, G. F. Pedersen, and Z. Ying, "User effects on the circular polarization of 5G mobile terminal antennas," *IEEE Transactions on Antennas and Propagation*, vol. 66, no. 9, pp. 4906–4911, Jun. 2018.

[4] J. Hejselbk, J. O. Nielsen, W. Fan, and G. F. Pedersen, "Measured 21.5 GHz indoor channels with user-held handset antenna array," *IEEE Transactions on Antennas and Propagation*, vol. 65, no. 12, pp. 6574–6583, Dec 2017.

[5] K. Zhao, Z. Ying, S. Zhang, and G. Pedersen, "User body effects on mobile antennas and wireless systems of 5G communication," in *2020 14th European Conference on Antennas and Propagation (EuCAP)*, Mar. 2020, pp. 1–5.

[6] L. Vähä-Savo, C. Cziezerski, M. Heino, K. Haneda, C. Icheln, A. Hazmi, and R. Tian, "Empirical evaluation of a 28 GHz antenna array on a 5G mobile phone using a body phantom," *IEEE Transactions on Antennas and Propagation*, vol. 69, no. 11, pp. 7476–7485, Nov. 2021.

[7] P. Liu, I. Syrytsin, J. Ødum Nielsen, G. Frølund Pedersen, and S. Zhang, "Characterization and modeling of the user blockage for 5G handset antennas," *IEEE Transactions on Instrumentation and Measurement*, vol. 70, pp. 1–11, Nov. 2021.

[8] C. Ballesteros, L. Vähä-Savo, K. Haneda, C. Icheln, J. Romeu, and L. Jofre, "Assessment of mmwave handset arrays in the presence of the user body," *IEEE Antennas and Wireless Propagation Letters*, vol. 20, no. 9, pp. 1736–1740, Jul. 2021.

[9] M. Heino, C. Icheln, and K. Haneda, "Finger effect on 60 GHz user device antennas," in *2016 10th European Conference on Antennas and Propagation (EuCAP)*, Apr. 2016, pp. 1–5.

[10] T. Q. K. Nguyen, M. S. Miah, L. Lizzi, K. Haneda, and F. Ferrero, "Experimental evaluation of user's finger effects on a 5G terminal antenna array at 26 GHz," *IEEE Antennas and Wireless Propagation Letters*, vol. 19, no. 6, pp. 892–896, Jun. 2020.

[11] V. Raghavan, V. Podshivalov, J. Hulten, M. A. Tassoudji, A. Sampath, O. H. Koymen, and J. Li, "Spatio-temporal impact of hand and body blockage for millimeter-wave user equipment design at 28 GHz," *IEEE Communications Magazine*, vol. 56, no. 12, pp. 46–52, Dec. 2018.

[12] S. S. Zhekov, O. Franek, and G. F. Pedersen, "Dielectric properties of human hand tissue for handheld devices testing," *IEEE Access*, vol. 7, pp. 61 949–61 959, May 2019.

[13] V. Raghavan, M.-L. Chi, M. A. Tassoudji, O. H. Koymen, and J. Li, "Antenna placement and performance tradeoffs with hand blockage in millimeter wave systems," *IEEE Transactions on Communications*, vol. 67, no. 4, pp. 3082–3096, Apr. 2019.

[14] V. Raghavan, S. Noimanivone, S. K. Rho, B. Farin, P. Connor, R. A. Motos, Y.-C. Ou, K. Ravid, M. A. Tassoudji, O. H. Koymen, and J. Li, "Hand and body blockage measurements with form-factor user equipment at 28 GHz," *IEEE Transactions on Antennas and Propagation*, vol. 70, no. 1, pp. 607–620, Jan. 2022.

[15] 3rd Generation Partnership Project (3GPP), "Discussion of mmwave ue eirp and eis test," *3GPP TSG-RAN WG4 NR AH Meeting R4-1700095*, Jan. 2017.